Journal
Proceedings of the National Academy of Sciences of the United States of America, 114(21)

ISSN
0027-8424

Authors
Rosa, PFS
Kang, J
Luo, Yongkang
et al.

Publication Date
2017-05-23

DOI
10.1073/pnas.1703016114

Competing magnetic orders in the superconducting state of Nd-doped $CeRhIn_5$ under pressure

P. F. S. Rosa[1], Jian Kang[3], Yongkang Luo[1], N. Wakeham[1], E. D. Bauer[1], F. Ronning[1], Z. Fisk[2], R. M. Fernandes[3] and J. D. Thompson[1]
[1] *Los Alamos National Laboratory. Los Alamos, New Mexico 87545, U.S.A.*
[2] *University of California, Irvine, California 92697-4574, U.S.A.*
[3] *School of Physics and Astronomy, University of Minnesota, Minneapolis, Minnesota 55455, USA*
(Dated: September 14, 2021)

Applied pressure drives the heavy-fermion antiferromagnet $CeRhIn_5$ towards a quantum critical point that becomes hidden by a dome of unconventional superconductivity. Magnetic fields suppress this superconducting dome, unveiling the quantum phase transition of local character. Here, we show that 5% magnetic substitution at the Ce site in $CeRhIn_5$, either by Nd or Gd, induces a zero-field magnetic instability inside the superconducting state. This magnetic state not only should have a different ordering vector than the high-field local-moment magnetic state, but it also competes with the latter, suggesting that a spin-density-wave phase is stabilized in zero field by Nd and Gd impurities – similarly to the case of $Ce_{0.95}Nd_{0.05}CoIn_5$. Supported by model calculations, we attribute this spin-density wave instability to a magnetic-impurity driven condensation of the spin excitons that form inside the unconventional superconducting state.

Unconventional superconductivity (SC) frequently is found as an antiferromagnetic (AFM) transition is tuned by chemical substitution or pressure toward a zero-temperature phase transition, a magnetic quantum-critical point. This observation has a qualitative explanation: the proliferation of quantum fluctuations of magnetic origin at low temperatures can trigger the formation of a new ordered state. Unconventional superconductivity is a natural candidate state because it can be induced by an attractive Cooper-pair interaction provided by the fluctuating magnetism [1, 2]. Typical examples include copper-oxides, which without chemical substitution are AFM Mott insulators [3], metallic iron-based antiferromagnets that superconduct under pressure or with chemical substitutions [4], and rare-earth heavy-fermion compounds with large effective electronic masses [5].

A characteristic manifestation of the unconventional nature of the superconducting state is the momentum dependence of the SC gap Δ that develops below the superconducting transition temperature (T_c). In contrast to conventional superconductors, Δ is not uniform but instead has different signs in different regions of the Fermi surface. Despite the distinct chemical and electronic properties of these materials, the interplay between magnetism and SC is common among them, calling for a deep understanding of this relationship. In this regard, heavy-fermion materials offer an ideal platform to explore the relationship between these two phases.

An additional common feature among these different classes of superconductors is the emergence of a collective magnetic excitation below T_c often attributed to the formation of a spin exciton [6]. This collective mode, whose energy has been shown to scale with Δ across different materials [7], is a direct consequence of the sign-changing nature of Δ. An example is the heavy-fermion superconductor $CeCoIn_5$, known to be very close to an AFM quantum-critical point without tuning [5]. Indeed, its SC gap is sign-changing [8, 9] and a spin resonance mode is observed below T_c [10]. The energy of this mode in $CeCoIn_5$ scales with its SC gap with the same proportionality found in copper-oxide and iron-based systems.

Recent inelastic neutron scattering experiments find that the resonance mode in $CeCoIn_5$ is incommensurate at the wavevector $\mathbf{Q} = (0.45, 0.45, 0.5)$ [11]. Due to Ce's $4f$ crystal-field environment, this mode is a doublet and the corresponding fluctuations are polarized along the c-axis . When a magnetic field H is applied in the tetragonal ab-plane, this mode splits into two well-defined branches [12, 13]. The field dependence of the Zeeman-split lower energy mode extrapolates to zero energy at ~ 110 kOe, which is remarkably close to the field where long-range AFM order develops inside the low-T, high-H SC state [14–16]. Spin-density wave (SDW) order in this so-called Q-phase has a small c-axis ordered moment of $0.15\ \mu_B$, which corresponds closely to the spectral weight of the low-energy resonance mode. Moreover, the SDW displays the same incommensurate wave-vector $\mathbf{Q}$ as the spin resonance mode [15]. These observations suggest that the Q-phase is the result of a condensation of spin excitations [11, 13, 17].

In addition to the field-induced Q-phase, AFM order is found in $Ce_{0.95}Nd_{0.05}CoIn_5$ below T_c, in this case at zero field [18]. The wave-vector and moment size of the Nd-induced magnetism are the same as those observed in the Q-phase of $CeCoIn_5$ [19]. Although the sign-changing Δ, with its nodes on the Fermi surface, plays a non-trivial role in enabling these orders, the obvious similarity between H- and Nd-induced magnetism strongly suggests that they have a common origin, namely condensation of the spin excitations that give rise to the resonance mode.

No evidence for the Q-phase has been found in other $CeMIn_5$ members (M = Rh, Ir) or, for that matter, in any other superconductor. It is uncommon to find a magnetic transition below T_c when both superconducting and magnetic states arise from the same electrons. Besides the example of $CeCoIn_5$, field-induced magnetism has been observed in $La_{1.9}Sr_{0.1}CuO_4$ [20, 21]. This AFM order, however, is distinct from a Q-like phase and is closely related to the field-induced magnetism in the SC state of pressurized $CeRhIn_5$ [22]. At zero pressure, $CeRhIn_5$ displays AFM order at $T_N = 3.8$ K and $\mathbf{Q}_{\mathrm{AFM}} = (0.5, 0.5, 0.297)$ [23]. Pressurizing $CeRhIn_5$ tunes its magnetic transition toward a quantum-critical point and induces SC that coexists with AFM order for pressures up to $P_{c1} = 1.75$ GPa, where T_c equals T_N. Above P_{c1}, evidence for T_N is absent and only SC is observed [22, 24, 25]. Application of a magnetic field, however, induces magnetism in the SC state between P_{c1} and the quantum-critical point at $P_{c2} \sim 2.3$ GPa [22, 26]. Unlike magnetic order in the Q-phase, which exists only inside the SC state, field-induced magnetism in $CeRhIn_5$ persists into the normal state above the Pauli-limited H_{c2} and is a smooth continuation of the zero-field $T_N(P)$ boundary [22, 26]. This magnetism may obscure or preempt the formation of a Q-like phase, but strong similarities of $CeCoIn_5$ to $CeRhIn_5$ at $P > P_{c1}$ [22, 27] suggest the possibility that AFM order might develop in the high pressure SC state of $Ce_{1-x}Nd_xRhIn_5$ in zero field.

In this paper, we show that Nd induces a zero-field phase transition in the high-pressure SC phase of $Ce_{0.95}Nd_{0.05}RhIn_5$ and present evidence that the phase transition is due to magnetic order. This result generalizes the observation of magnetic order below T_c in $Ce_{0.95}Nd_{0.05}CoIn_5$ because pressure suppresses the magnetic order at the same rate in both compounds. Our model calculations support our conclusion that the magnetism in Nd-doped $CeRhIn_5$ is due to the condensation of spin excitations promoted by magnetic impurity scattering, and is thus distinct from the local-moment magnetism in pure $CeRhIn_5$ promoted by the application of magnetic fields. In agreement with this proposal, we observe a competition between the field-induced magnetism, which displays the same behavior as in $CeRhIn_5$, and the Nd-induced magnetism in zero field. Hence, we expect a spin resonance with c-axis character below T_c in $CeRhIn_5$ at pressures greater than P_{c1}. More generally, our work reveals a route to induce zero-field magnetic order via chemical substitution of magnetic impurities in other unconventional superconductors that host spin resonance modes.

I. RESULTS

For comparison with $Ce_{0.95}Nd_{0.05}CoIn_5$, we grew crystals of $Ce_{0.95}Nd_{0.05}RhIn_5$ by an In-flux technique [28] and studied its pressure and field dependence by electrical resistivity and AC calorimetry measurements (See Methods for details). Figure 1a shows the low-temperature electrical resistivity, $\rho(T)$, on sample s1 at representative pressures, and the inset displays $\rho(T)$ in the whole T-range. Although Nd-substitution reduces $T_N(P=0)$ from 3.8 K to 3.4 K and slightly increases the residual resistivity ρ_0 to 0.2 $\mu\Omega.cm$, the P-dependence reported in Fig. 1a is essentially identical to that of $CeRhIn_5$ below $P^*_{c1} = 1.8$ GPa where T_c equals T_N. We also note that, at zero pressure, the $H-T$ phase diagram of $Ce_{0.95}Nd_{0.05}RhIn_5$ closely resembles the one found in $CeRhIn_5$. These results indicate that 5% Nd does not change drastically the local AFM character of T_N below P^*_{c1}. Once T_c exceeds T_N at P^*_{c1}, there is no evidence for magnetism in $\rho(T)$, and the possibility of Nd-induced magnetism is obscured by the zero-resistance state below T_c. To investigate whether there is AFM order in the SC state, heat capacity measurements are necessary.

Figure 1b shows the T-dependence of heat capacity divided by temperature (C_{ac}/T) for sample s2 at various pressures. At ambient pressure, C_{ac}/T peaks at T_N as in $CeRhIn_5$. As T is lowered further, however, C_{ac}/T turns up below ~ 1 K, which was not observed in $CeRhIn_5$ [30]. This upturn is presumably associated with the nuclear moment of Nd ions, and it can be fit well by a sum of electronic ($\propto \gamma$) and nuclear ($\propto T^{-3}$) terms [31]. The inset of Fig. 1b shows that $C_{ac}T^2$ is linear in T^3, consistent with the presence of a nuclear Schottky contribution. We note, however, that an upturn also is observed at 2.3 GPa (not shown) where magnetic order is absent, suggesting that the hyperfine field may not be solely responsible for splitting the nuclear levels. Although Nd nuclei have large zero-field quadrupole moments, Kondo-hole physics cannot be ruled out as a possible source of the upturn [32, 33].

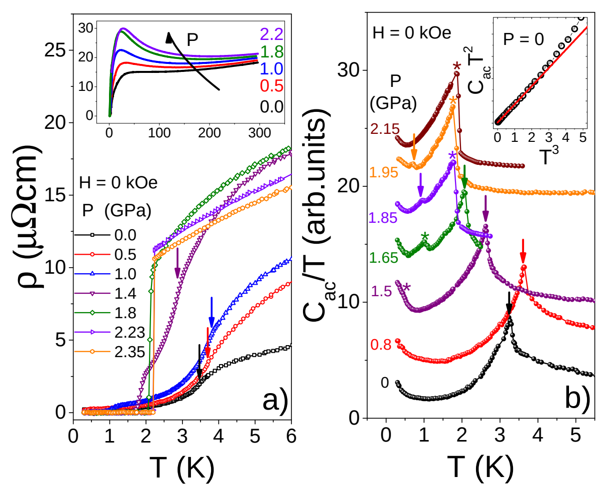

FIG. 1. a) Low-T dependence of the in-plane electrical resistivity, $\rho(T)$, of $Ce_{0.95}Nd_{0.05}RhIn_5$ (s1) under pressure. Arrows mark T_N determined by peaks in the first derivative. The inset shows $\rho(T)$ over the entire T-range. b) C_{ac}/T *vs* T for $Ce_{0.95}Nd_{0.05}RhIn_5$ (s2) under pressure. A vertical offset of 2.5 units is added for clarity. Arrows (asterisks) denote T_N (T_c). Inset shows a linear fit in a $C_{ac}T^2$ *vs* T^3 plot.

For pressures below P^*_{c1}, T_N evolves with P as it does in transport data. Evidence for bulk SC (marked by asterisks), however, is observed at lower temperatures relative to the zero-resistance state in $\rho(T)$. A difference between zero-resistance and bulk SC transitions also appears in $CeRhIn_5$ and has been attributed to filamentary SC due to the presence of long-range AFM order [34]. Unlike $CeRhIn_5$ at pressures greater than P_{c1}, however, there is evidence for a phase transition in the SC state of $Ce_{0.95}Nd_{0.05}RhIn_5$ without an applied field. At 1.85 GPa, an anomaly in C_{ac}/T is observed at 1 K (arrow in Fig. 1b), below the SC transition at $T_c = 1.77$ K. For reasons discussed below, this anomaly stems from a magnetic order, and it is fundamentally different from the AFM order displayed by the system for pressures smaller than P_{c1}. The shape and magnitude of the anomaly relative to that at T_c are very similar to those at T_N in $Ce_{0.95}Nd_{0.05}CoIn_5$ (see Supplemental Materials), and the small entropy associated with it suggests that the magnetic order is most likely a small-moment density wave. As we will come to later, this evidence is most obvious in data shown in Fig. 3.

We summarize the zero-field results discussed above in the T-P phase diagram shown in Fig. 2. Local-moment-like AFM order coexists with bulk SC in a narrow pressure range below P^*_{c1}. From just below to just above P^*_{c1}, $T_N(P)$ changes discontinuously, in contrast to field-induced magnetism in $CeRhIn_5$, which is a smooth continuation of $T_N(P)$ from below P_{c1} [22]. This supports the interpretation that H- and Nd-induced magnetic orders have different origins. Therefore, the Nd-induced transition is labeled T_N^{Nd} to distinguish it from T_N in pure $CeRhIn_5$. Above P^*_{c1}, T_N^{Nd} is suppressed at a rate of -2.4 K/GPa and extrapolates to zero temperature, i.e. a quantum-critical point, at $P^*_{c2} \sim 2.3$ GPa inside the superconducting phase. Whether the coincidence of P^*_{c2} and P_{c2} is accidental or not requires further investigation beyond the scope of our work. As shown in the Supplemental Materials, the rate of suppression of this Nd-induced transition is the same rate found in $Ce_{0.95}Nd_{0.05}CoIn_5$ within experimental uncertainty, strongly indicating a common origin. Because entropy associated with the zero-field transition is rather small, as found in $Ce_{1-x}Nd_xCoIn_5$, the typical signature of quantum criticality (i.e., divergence of C/T at low-T) is likely hidden by SC and by the upturn in C/T. We also note that the highest T_c achieved in $Ce_{0.95}Nd_{0.05}RhIn_5$, $T_c^{\max} = 1.85$ K, is 0.4 K lower than $T_c^{\max}$ of $CeRhIn_5$. This same suppression of $T_c^{\max}$ is observed in $Ce_{0.95}Nd_{0.05}CoIn_5$ and indicates that Nd ions act similarly as magnetic pair-breaking impurities.

To further investigate the nature of the Nd-induced magnetism, we turn to the field-dependent heat capacity data. Figure 3a shows C_{ac}/T *vs* T at 1.85 GPa ($> P_{c1}$) and low magnetic fields. The zero-field transition at $T_N^{\mathrm{Nd}} = 0.96$ K remains unchanged in a field of 2.5 kOe. As the field is increased further, however, the specific heat anomaly splits, one anomaly moving to lower temperatures and the other to higher temperatures. At 11 kOe, our data show features at 1 K and 0.7 K. Previous reports on $CeRhIn_5$ at similar pressures (~ 1.9 GPa) show that the field-induced transition emerges at $T_N = 1$ K when $H = 11$ kOe [34]. It is thus reasonable to associate the anomaly we observe at 1 K and 11 kOe with the field-induced magnetism in $CeRhIn_5$. Further, Fig. 3b shows the high-H evolution of T_N with a field dependence very similar to that of $CeRhIn_5$: T_N first increases with H and then remains constant above the upper critical field H_{c2}. As shown in the $H-T$ phase diagram (Fig. 3c), this field-induced T_N clearly competes with T_N^{Nd}, as reflected in the rapid suppression of T_N^{Nd} as a function of H. In fact, no evidence for T_N^{Nd} is observed at fields $H \geq 22$ kOe, implying a field-induced quantum-critical point in addition to the pressure-induced, zero-field critical point of this order. Due to the reasons explained above, our results strongly point to two distinct types of magnetism emerging in $Ce_{0.95}Nd_{0.05}RhIn_5$. The first one is due to Nd ions and it has the hallmarks of that in $Ce_{0.95}Nd_{0.05}CoIn_5$. The second is the H-induced magnetism that appears in pure $CeRhIn_5$ [22, 26].

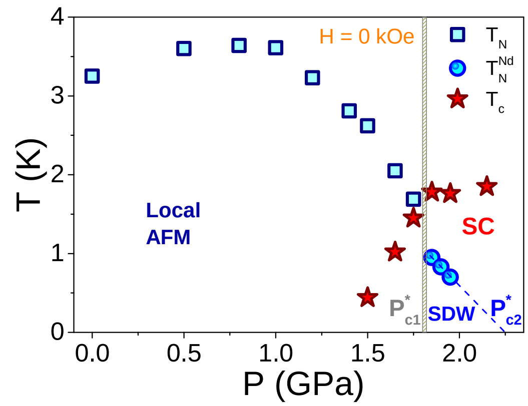

FIG. 2. Zero-field $T-P$ phase diagram of $Ce_{0.95}Nd_{0.05}RhIn_5$ (s2) obtained from AC calorimetry measurements. Here $P^*_{c1} \sim 1.8$ GPa and $P^*_{c2} \sim 2.3$ GPa.

II. DISCUSSION

What is the role of Nd and why is it special? At a concentration of 5%, average spacing of 17 Å and non-periodic distribution on Ce-sites, Nd is too dilute to induce magnetic order by dipole or indirect Ruderman-Kittel-Kasuya-Yosida interactions. Its role, then, must be more subtle. Using the bulk modulus of $CeRhIn_5$ and the unit-cell volume variation in $Ce_{1-x}Nd_xRhIn_5$, we estimate that $Ce_{0.95}Nd_{0.05}RhIn_5$ experiences an effective chemical pressure of $\Delta P = 0.25$ GPa relative to $CeRhIn_5$ [28]. From the phase diagram of $CeRhIn_5$, this ΔP would increase T_N by 0.1 K instead of producing the observed reduction. Hence, we conclude that chemical pressure *perse* is not the dominant tuning parameter.

The disruption of translational periodicity of the Ce lattice by Nd substitution creates a "Kondo hole" that

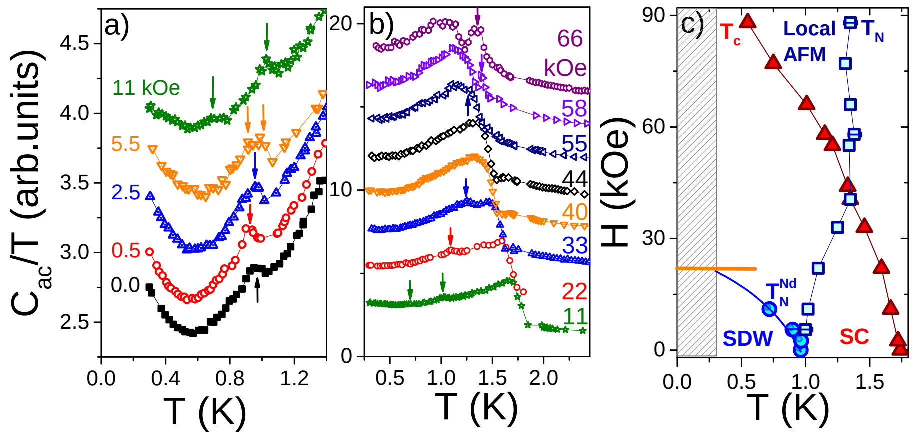

FIG. 3. AC heat capacity, C_{ac}, of $\mathrm{Ce_{0.95}Nd_{0.05}RhIn_5}$ (s2) at 1.85 GPa. a) T-dependence of C_{ac}/T at low fields. An offset of 0.2 has been added for clarity. b) T-dependence of C_{ac}/T at high fields. c) $H-T$ phase diagram. The diagonal bars delimit the inaccessible temperature region in our experiments ($T < 0.3$ K). The solid horizontal line at $H = 22$ kOe indicates that no transition is observed above 0.3 K for this field.

contributes to reducing T_N at zero pressure [28]. The latter conclusion is supported by the observation that non-magnetic La substitution for Ce in $\mathrm{CeRhIn_5}$ also depresses T_N similarly [32, 35]. Neodymium, however, carries an additional magnetic moment that is unlikely to be quenched by Kondo screening. In the context of $\mathrm{CeCoIn_5}$, Michal and Mineev [17] proposed that the Q-phase observed in the presence of an in-plane magnetic field is the consequence of the condensation of the spin-exciton collective mode found in the SC phase. Thus, it is natural to consider whether the Nd magnetic moments immersed in $\mathrm{CeRhIn_5}$ at zero field could also promote a similar behavior.

As discussed in detail in the Supplemental Materials, condensation of spin excitons takes place when the spin-resonance-mode frequency ω_{res} vanishes. Within an random phase approximation (RPA) approach, the latter is given by the pole of the renormalized magnetic susceptibility, i.e. when $\chi_{\mathrm{AFM}}(\mathbf{Q}, \omega_{\mathrm{res}}) = 1/U$, where U is the effective electronic interaction projected in the SDW channel and $\chi_{\mathrm{AFM}}(\mathbf{Q}, \omega_{\mathrm{res}})$ is the non-interacting magnetic susceptibility inside the SC state. When the ordering vector $\mathbf{Q}$ connects points of the Fermi surface with different signs of the SC gap, $\Delta_{\mathbf{k}} = -\Delta_{\mathbf{k}+\mathbf{Q}}$, $\chi_{\mathrm{AFM}}(\mathbf{Q}, \omega)$ generically diverges when $\omega \to 2\Delta$ and remains non-zero when $\omega \to 0$. Thus, even a very weak U can in principle induce a resonance mode with frequency near 2Δ. Once the interaction increases, ω_{res} moves to lower frequencies. When the interaction overcomes a critical value, $U > U_c \equiv \chi^{-1}_{\mathrm{AFM}}(\mathbf{Q}, 0)$, the resonance mode vanishes and SDW order is established inside the SC dome.

In our case, the interaction U is presumably independent of pressure. Thus, in order for magnetic impurities to promote spin-exciton condensation, $\chi_{\mathrm{AFM}}(\mathbf{Q}, 0)$ must increase (i.e. the critical interaction value U_c must decrease) as function of the impurity potential. To investigate whether this is a sensible scenario, we considered a toy model consisting of two "hot spots" located at momenta $\mathbf{k}$ and $\mathbf{k}+\mathbf{Q}$ at the Fermi surface such that $\Delta_{\mathbf{k}} = -\Delta_{\mathbf{k}+\mathbf{Q}}$. Note that such a hot-spots model has been previously employed to study the effects of disorder on SC [38]. To focus on the general properties of the model, we linearize the band dispersion around the hot spots and compute both $\chi_{\mathrm{AFM}}(\mathbf{Q}, 0)$ and the effective gap amplitude Δ at $T = 0$ as function of the total impurity scattering rate τ^{-1} within the self-consistent Born approximation (similarly to what was done in Ref. [39] for s^{+-} SC and perfectly nested bands). As shown in Figure 4, whereas both magnetic and non-magnetic impurity scattering suppress Δ at the same rate (panel 4b),

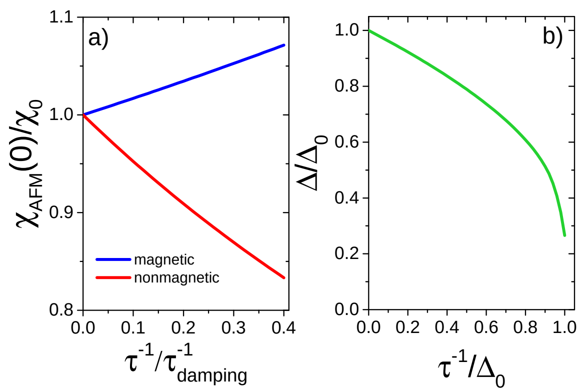

FIG. 4. a) Static spin susceptibility $\chi_{\mathrm{AFM}}(\mathbf{Q}, \omega = 0)$ as function of the total impurity scattering rate for the cases of non-magnetic (red curve) and paramagnetic impurities (blue curve). b) The suppression of the effective SC gap Δ by both magnetic and non-magnetic impurities. In these plots, we considered point-like impurities. Here, Δ_0 is the gap of the clean system whereas $\tau^{-1}_{\mathrm{damping}}$ is the Landau damping (see Supplemental Materials for details).

we find that $\chi_{\mathrm{AFM}}(\mathbf{Q},0)$ is suppressed for non-magnetic impurity but enhanced by magnetic impurity scattering (panel 4a). Thus, in the case of non-magnetic impurities, athough the resonance mode frequency may decrease as compared to the clean case, it never collapses to zero. Because magnetic impurity scattering enhances $\chi_{\mathrm{AFM}}(\mathbf{Q},0)$ but not necessarily destroys SC, the system may undergo an SDW transition inside the SC dome. Although the fate of the system will depend on microscopic details beyond those captured by the toy model considered here, our model nicely illustrates that it is plausible for magnetic impurity scattering to drive spin-exciton condensation in the SC phase. In this regard, we note that previous investigations of a microscopically-motivated theoretical model also found that the Q-phase may be stabilized by magnetic impurities even at zero external field [40].

These results suggest that other magnetic impurities could induce the same type of SDW order in both $CeCoIn_5$ and pressurized $CeRhIn_5$. In fact, we show in the Supplemental Materials that easy-plane Gd^{3+} ions ($J = S = 7/2$) also induce a transition in the heat capacity data of both Co and Rh members. This anomaly is similar to the one induced by easy-axis (c-axis) Nd^{3+} ions ($J = 9/2$, $L = 3$, $S = 3/2$) discussed above. Hence, Nd is not "special" in inducing magnetic order in the superconducting states of $Ce_{0.95}Nd_{0.05}CoIn_5$ and $Ce_{0.95}Nd_{0.05}RhIn_5$, and other unconventional superconductors that host a spin resonance mode may also display zero-field magnetism via the same mechanism. Our results also imply that non-magnetic impurities will not induce condensation of excitations, in agreement with experimental data on La-substituted $CeRhIn_5$ [35, 41, 42].

Finally, we note that the SDW ordering vector in Nd-doped $CeCoIn_5$ corresponds closely to the nodal structure [11] that is also found in the superconducting state of $CeRhIn_5$ [37]. Hence, the magnetic wave-vector of zero-field order above P^*_{c1} in $Ce_{0.95}Nd_{0.05}RhIn_5$ should also be close to $\mathbf{Q}= (0.45, 0.45, 0.5)$, and we expect neutron scattering experiments to find a spin resonance of c-axis character below T_c in $CeRhIn_5$ at $P > P_{c1}$.

III. CONCLUSION

In summary, we generalize the observation of Nd-induced magnetism in $CeCoIn_5$ to pressurized $CeRhIn_5$ and Gd-substituted members. This spin-density wave order, which reflects the nodal-gap symmetry, is argued to be a consequence of the condensation of spin excitations that arise inside the SC state. Given the several similarities between $CeCoIn_5$ and Ce_2PdIn_8 [43], Nd substitution might nucleate AFM order in its superconducting state. Appropriate substitutions in other unconventional superconductors that host a spin resonance also should induce zero-field magnetism by the same mechanism, and magnetism should be tunable to a quantum-critical point inside their SC phase.

We thank A. V. Chubukov, H. Löhneysen, S. Maiti, and P. G. Pagliuso for useful discussions. Work at Los Alamos by Y.L., N.W., E.D.B., F.R., and J.D.T. was performed under the auspices of the U.S. Department of Energy, Office of Basic Energy Sciences, Division of Materials Science and Engineering. P. F. S. R. acknowledges a Director's Postdoctoral Fellowship through the LANL LDRD program. The theoretical work (J.K. and R.M.F.) was supported by the U.S. Department of Energy, Office of Science, Basic Energy Sciences, under Award number DE-SC0012336.

Methods

The series $Ce_{1-x}Nd_xRhIn_5$ was grown by the In-flux technique and its properties are reported elsewhere [28]. Crystals with x=0.05 and free of unreacted In were mounted in a hybrid piston-cylinder pressure cell, filled with silicone fluid as the pressure medium, and a piece of Pb whose change in T_c served as a manometer. Gd-substituted crystals were grown using the same method. Electrical resistivity was measured by a four-probe method with current flow in the ab-plane. Semi-quantitative heat capacity was obtained by an AC calorimetry technique described elsewhere [29]. Magnetic fields to 9 T were applied parallel to the ab-plane. The results above have been reproduced in different crystals and, for clarity, we show resistivity and calorimetry data for two representative samples labeled sample 1 (s1) and sample 2 (s2), respectively.

[1] Monthoux P, Pines D & Lonzarich GG (2007) Superconductivity without phonons. Nature 450, 1177-1183.
[2] Scalapino DJ (2012) A common thread: The pairing interaction for unconventional superconductors. Rev. Mod. Phys. 84, 1383.
[3] Schilling A, Cantoni M, Guo JD & Ott HR (1993) Superconductivity above 130 K in the Hg-Ba-Ca-Cu-O system. *Nature* 363, 56.
[4] Stewart GR. Superconductivity in iron compounds (2011) *Rev. Mod. Phys.* **83**, 1589.
[5] White BD, Thompson JD, Maple MB (2015) Unconventional superconductivity in heavy-fermion compounds. *Physica C* **514**, 246.
[6] for a review, see M. Eschrig, Adv. Phys. 55, 47 (2006).
[7] Yu G, Li Y, Motoyama EM & Greven, M (2009) A universal relationship between magnetic resonance and super-

conducting gap in unconventional superconductors. *Nat. Phys.* **5**, 873.

[8] Park WK, Sarrao JL, Thompson JD, and Greene LH (2008) Andreev Reflection in Heavy-Fermion Superconductors and Order Parameter Symmetry in $CeCoIn_5$. Phys. Rev. Lett. 100, 177001.

[9] Zhou BB, *et al.* (2013) Visualizing nodal heavy fermion superconductivity in $CeCoIn_5$. Nature Phys. 9, 474.

[10] Stock C, Broholm C, Hudis J, Kang H J & Petrovic C (2008) Spin resonance in the d-Wave superconductor $CeCoIn_5$. *Phys. Rev. Lett.* **100**, 087001.

[11] Raymond S & Lapertot G (2015) Ising incommensurate spin resonance of $CeCoIn_5$: A Dynamical Precursor of the Q phase. *Phys. Rev. Lett.* **115**, 037001.

[12] Panarin J, Raymond S, Lapertot G & Flouquet J (2009) Evolution of the spin resonance in $CeCoIn_5$ under magnetic field. *J. Phys. Soc. Jpn.* **78**, 113706.

[13] Stock C, Broholm C, Zhao Y, Demmel F, Kang HJ, Rule KC & Petrovic C (2012) Magnetic field splitting of the spin resonance in $CeCoIn_5$. *Phys. Rev. Lett.* **109**, 167207.

[14] Young BL, *et al.* (2007) Microscopic Evidence for Field-Induced Magnetism in $CeCoIn_5$. *Phys. Rev. Lett.* **98**, 036402.

[15] Kenzelmann M, *et al.* (2008) Coupled superconducting and magnetic order in $CeCoIn_5$. *Science* **321**, 1652.

[16] Kenzelmann M, *et al.* (2010) Evidence for a magnetically driven superconducting Q phase of $CeCoIn_5$. *Phys. Rev. Lett.* **104**, 127001.

[17] Michal VP & Mineev VP (2011) Field-induced spin-exciton condensation in the $d_{x^2-y^2}$-wave superconductor $CeCoIn_5$. *Phys. Rev. B* **84**, 052508.

[18] Hu R, Lee Y, Hudis J, Mitrovic VF & Petrovic C (2008) Composition and field-tuned magnetism and superconductivity in $Nd_{1-x}Ce_xCoIn_5$. *Phys. Rev. B* **77**, 165129.

[19] Raymond S, Ramos SM, Aoki D, Knebel G, Mineev VP & Lapertot G (2014) Magnetic order in $Ce_{0.95}Nd_{0.05}CoIn_5$: The Q-phase at zero magnetic field. *J. Phys. Soc. Jpn.* **83**, 013707.

[20] Lake B, *et al.* (2002) Antiferromagnetic order induced by an applied magnetic field in a high-temperature superconductor. *Nature* **415**, 299.

[21] Demler E, Sachdev S & Zhang Y (2011) Spin-ordering quantum transitions of superconductors in a magnetic field. *Phys. Rev. Lett.* **87**, 067202.

[22] Park T, *et al.* (2006) Hidden magnetism and quantum criticality in the heavy fermion superconductor $CeRhIn_5$. *Nature* **440**, 65-68.

[23] Bao W, *et al.* (2000) Incommensurate magnetic structure of $CeRhIn_5$. Phys. Rev. B 62, R14621(R).

[24] Hegger H, *et al.* (2000) Pressure-induced superconductivity in quasi-2D $CeRhIn_5$. *Phys. Rev. Lett.* **84**, 4986.

[25] Mito T, *et al.* (2003) Coexistence of antiferromagnetism and superconductivity near the quantum criticality of the heavy-fermion compound $CeRhIn_5$. *Phys. Rev. Lett.* **90**, 077004.

[26] Knebel G, Aoki D, Braithwaite D, Salce B & Flouquet J (2006) Coexistence of antiferromagnetism and superconductivity in $CeRhIn_5$ under high pressure and magnetic field. *Phys. Rev. B* **74**, 020501(R).

[27] Pham LD, Park T, Maquilon S, Thompson JD & Fisk Z (2006) Reversible Tuning of the Heavy-Fermion Ground State in $CeCoIn_5$. Phys. Rev. Lett. 97, 056404.

[28] Rosa PFS, Oostra A, Thompson JD, Pagliuso PG & Fisk Z (2016) Unusual Kondo-hole effect and crystal-field frustration in Nd-doped $CeRhIn_5$. *Phys. Rev. B* 94, 045101.

[29] Sidorov VA, Thompson JD & Fisk Z (2010) Magnetic transitions in a heavy-fermion antiferromagnet U_2Zn_{17} at high pressure. *J. Phys.: Condens. Matter* **22**, 406002.

[30] We note that an upturn in C/T also has been observed in a commercial Quantum Design PPMS by means of quasiadiabatic thermal relaxation technique.

[31] Anderson AC, Holmstrom B, Krusius M & Pickett GR (1969) Calorimetric investigation of the hyperfine interactions in metallic Nd, Sm, and Dy. *Phys. Rev.* **183**, 546.

[32] Pagliuso PG, *et al.* (2002) Ce-site dilution studies in the antiferromagnetic heavy fermions $Ce_mRh_nIn_{3m+2n}$ ($m = 1, 2; n = 0, 1$). *Phys. Rev. B* **66**, 054433.

[33] Bauer ED, *et al.* (2011) Electronic inhomogeneity in a Kondo lattice. *Proc. Natl. Acad. Sci. USA* **108**, 6857

[34] Park T & Thompson JD (2009) Magnetism and superconductivity in strongly correlated $CeRhIn_5$. *New J. Phys.* **11**, 055062.

[35] Mendonça-Fereira L, *et al.* (2008) Tuning the Pressure-Induced Superconducting Phase in Doped $CeRhIn_5$. *Phys. Rev. Lett.* **101**, 017005.

[36] Pagliuso PG, *et al.* (2002) Structurally tuned superconductivity in heavy-fermion $CeMIn_5$ (M = Co, Ir, Rh). *Physica B* **320**, 370-375.

[37] Park T, Bauer ED, & Thompson JD (2008) Probing the nodal gap in the pressure-induced heavy fermion superconductor $CeRhIn_5$. *Phys. Rev. Lett.* **101** 177002.

[38] Kang J and Fernandes RM (2016)Robustness of quantum critical pairing against disorder. Phys. Rev. B **93**, 224514.

[39] Maiti S, Knolle J, Eremin I, and Chubukov AV (2011) Effect of nodes, ellipticity, and impurities on the spin resonance in iron-based superconductors. Phys. Rev. B **84**, 144524.

[40] Martiny JHJ, Gastiasoro MN, Vekhter I, and Andersen BM (2015) Impurity-induced antiferromagnetic order in Pauli-limited nodal superconductors: Application to heavy-fermion $CeCoIn_5$. Phys. Rev. B **92**, 224510.

[41] Panarin J, Raymond S, Lapertot G, Flouquet J, and Mignot JM (2011) Effects of nonmagnetic La impurities on the spin resonance of $Ce_{1-x}La_xCoIn_5$ single crystals as seen via inelastic neutron scattering. *Phys. Rev. B* **84**, 052505.

[42] Nakatsuji S, *et al.* (2002) Intersite coupling effects in a Kondo lattice. Phys. Rev. Lett. **89** 106402.

[43] Dong JK, *et al.* (2011) Field-induced quantum critical point and nodal superconductivity in the heavy-fermion superconductor Ce_2PdIn_8. *Phys. Rev. X* **1**, 011010.

Supplemental Materials

Competing magnetic orders in the superconducting state of heavy-fermion $CeRhIn_5$

IV. SUPPORTING AC CALORIMETRY MEASUREMENTS IN $CeCoIn_5$ AND $CeRhIn_5$

Single crystals of nominally $Ce_{0.95}Nd_{0.05}CoIn_5$ were grown from an excess In flux and characterized by pressure-dependent AC calorimetry, as described in the main text. These measurements were carried out in a pressure cell under conditions also discussed in the main text. Figure S1 shows C_{ac}/T as a function of T at two pressures. At atmospheric pressure (top curve), a pronounced peak in C_{ac}/T defines the superconducting transition temperature T_c =1.63 K that is followed at lower temperatures by an anomaly peaked near 0.7 K. These features in data at atmospheric pressure coincide well with those reported in ref. [15] (main text) and indicate that the nominal Nd content is very close to the actual content. Consequently, we associate the lower temperature anomaly with antiferromagnetic order at $T_N^{\rm Nd}$. We note that the shapes of the two anomalies resemble those found in $Ce_{0.95}Nd_{0.05}RhIn_5$. As shown in Fig. S1a, an applied pressure of only 0.13 GPa reduces $T_N^{\rm Nd}$ to $\sim$ 0.4 K. Assuming that $T_N^{\rm Nd}$ decreases linearly with P (Fig. S1a inset) gives d$T_N^{\rm Nd}$/dP ~ -2.3 K/GPa. This rate of decrease is very close to that found in Fig. 2 of the main text where, for $Ce_{0.95}Nd_{0.05}RhIn_5$ above P_{c1}, d$T_N^{\rm Nd}$/dP ~ -2.4 K/GPa. The fact that Nd-induced zero-field antiferromagnetic order in similarly doped $CeCoIn_5$ and $CeRhIn_5$ displays the same sensitivity to pressure strongly suggests that the zero-field magnetism has a common origin in both materials.

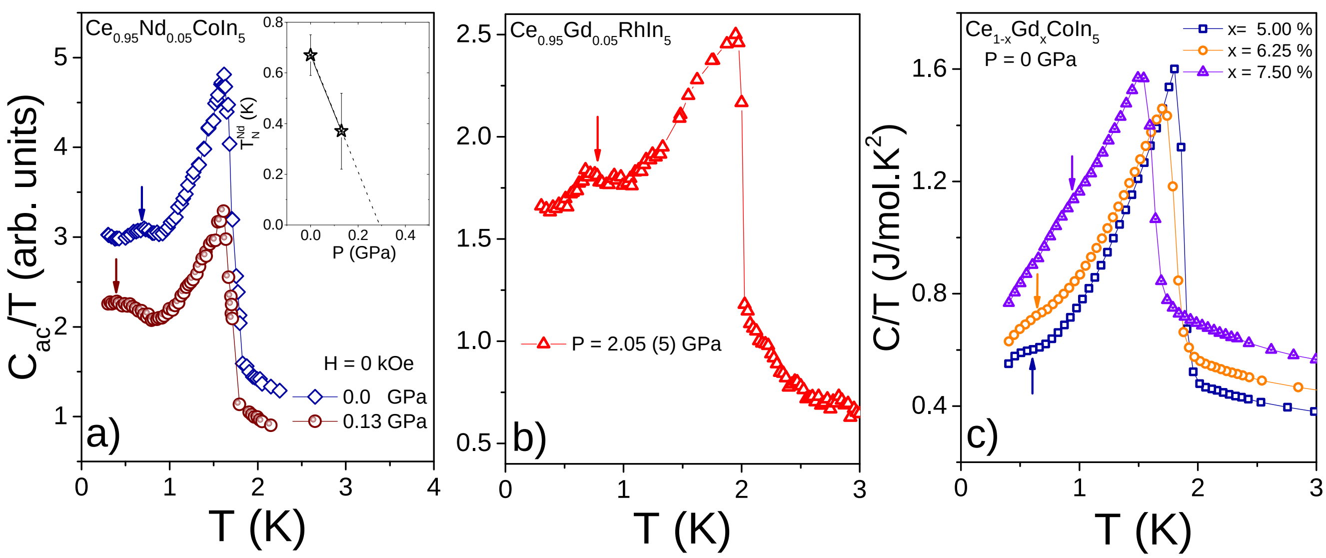

FIG. S1. (a) C_{ac}/T *vs* T of $Ce_{0.95}Nd_{0.05}CoIn_5$ at two pressures. Arrows show T_N and inset shows its extrapolation to $T = 0$. (b) C_{ac}/T *vs* T of $Ce_{0.95}Gd_{0.05}CoIn_5$ at 2.05 GPa. (c) C_{ac}/T *vs* T of $Ce_{1-x}Gd_xCoIn_5$ ($x = 0.05, 0.0625, 0.075$) at ambient pressure. The curves are shifted by 0.1 J/mol.K^2 for clarity. Arrows show T_N determined as the minimum in the first derivative of the data.

Single crystals of nominally $Ce_{0.95}Gd_{0.05}RhIn_5$ were grown from an excess In flux and characterized by pressure-dependent AC calorimetry, as described in the main text. Figure S1b shows C_{ac}/T as a function of T at 2.05 GPa. A pronounced peak in C_{ac}/T defines the superconducting transition temperature T_c =1.95 K that is followed at lower temperatures by an anomaly peaked near 0.7 K determined by the minimum in derivative of C/T.

Finally, single crystals of nominally $Ce_{1-x}Gd_xCoIn_5$ ($x = 0.05, 0.0625, 0.075$) were grown from an excess In flux and characterized by specific heat at ambient pressure in a commercial PPMS. Figure S1c shows C_{ac}/T as a function of T for all concentrations. A pronounced peak in C/T defines the superconducting transition temperature T_c = 1.8 K, 1.7 K, and 1.52 K that is followed at lower temperatures by an anomaly peaked near 0.6 K, 0.7 K, and 0.97 K.

V. IMPACT OF DISORDER ON THE MAGNETIC SUSCEPTIBILITY INSIDE THE SUPERCONDUCTING STATE

To gain insight into the problem, and keep the calculation analytically tractable, we employ the hot spots approximation. In particular, we consider two points on the Fermi surface, labeled c and d, separared by the SDW vector $\boldsymbol{Q}$, such that $\Delta_{\boldsymbol{k}} = -\Delta_{\boldsymbol{k}+\boldsymbol{Q}}$. Next, we linearize the dispersions around the hot spots

$$\epsilon_c(\boldsymbol{k}) = \boldsymbol{v}_c \cdot \boldsymbol{k} \ , \qquad \epsilon_d(\boldsymbol{k}+\boldsymbol{Q}) = \boldsymbol{v}_d \cdot \boldsymbol{k} \tag{1}$$

where the momentum $\boldsymbol{k}$ is measured with respect to $\boldsymbol{k}_F$ and $\boldsymbol{v}_{c/f}$ are the Fermi velocities. Here, we consider $v_c = v_d$ and let the relative angle between them be arbitrary but non-zero. The case $\boldsymbol{v}_c = -\boldsymbol{v}_d$ corresponds to perfect nesting, which was studied in Ref. [39]. Here, we focus on the case where nesting is not perfect. As long as the SDW instability is driven by the low-energy electronic states, the linearized approximation can be used to compute the leading contribution to the magnetic susceptibility.

There are two different types of impurity potentials: the non-magnetic potential $u_{\boldsymbol{k}}$, which couples to the charge degrees of freedom, and the paramagnetic potential $\mathbf{u}^p_{\boldsymbol{k}}$, which couples to the spin degrees of freedom. Each impurity potential can be split into small-momentum scattering, u_0 and $\mathbf{u}^p_0$ (which does not couple the fermions on the two hot spots), and large-momentum scattering $u_{\boldsymbol{Q}}$ and $\mathbf{u}^p_{\boldsymbol{Q}}$ (which couples the fermions on the two hot spots).

First, we study the impact of the various types of disorder on the pairing gap. Here, we assume the existence of a SC state, without discussing its origin. Thus, we consider a static pairing interaction V corresponding to a repulsive interaction coupling fermions from different hot spots, such that $\Delta_c = -\Delta_d$. To proceed, it is convenient to define Nambu spinors $\Psi^\dagger_{i\boldsymbol{k}} = \left(f^\dagger_{i,\boldsymbol{k}\uparrow},\, f_{i,-\boldsymbol{k}\downarrow}\right)$. The Green's function in Nambu space is then given by:

$$G_c^{-1} = Z_\omega^{-1}(i\omega_n\sigma_0 - \bar{\Delta}_\omega\sigma_1) - \epsilon_c(\boldsymbol{k})\sigma_3 \ , \qquad G_d^{-1} = Z_\omega^{-1}(i\omega_n\sigma_0 + \bar{\Delta}_\omega\sigma_1) - \epsilon_d(\boldsymbol{k})\sigma_3 \tag{2}$$

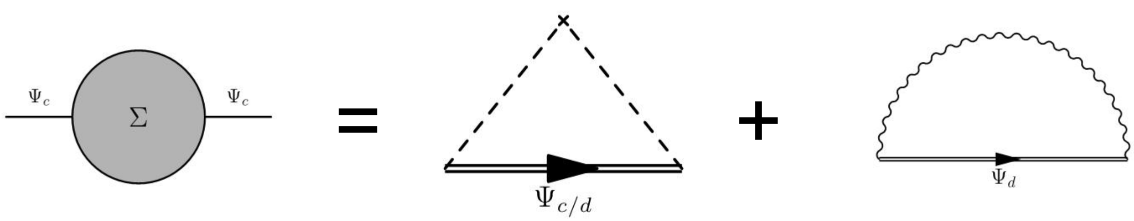

FIG. S2. The fermionic self energy in the self-consistent approximation. The two diagrams show the contributions arising from impurities and from the pairing interaction, respectively.

where Z_ω is the imaginary part of the normal component of the self-energy and $\bar{\Delta}_\omega$ (the gap normalized by impurities) is the real part of the anomalous component of the self-energy. As shown in Fig S2, the fermionic self-energy in the self-consistent approximation becomes, at $T = 0$

$$\begin{aligned}\Sigma_c(i\omega_n) = &-\pi\big(u_0^2 + u_{\boldsymbol{Q}}^2 + (u_0^p)^2 + (u_{\boldsymbol{Q}}^p)^2\big)N_f\frac{i\omega_n}{\sqrt{\omega_n^2+\bar{\Delta}_\omega^2}}\sigma_0 + \pi\big(u_0^2 - u_{\boldsymbol{Q}}^2 - (u_0^p)^2 + (u_{\boldsymbol{Q}}^p)^2\big)N_f\frac{\bar{\Delta}_\omega}{\sqrt{\omega_n^2+\bar{\Delta}_\omega^2}}\sigma_1\\ &+ VN_f\int_0^\Lambda \frac{\bar{\Delta}_\omega \mathrm{d}\omega}{\sqrt{\omega^2+\bar{\Delta}_\omega}}\sigma_1\end{aligned} \tag{3}$$

To solve for Z_ω and $\bar{\Delta}_\omega$, we average over impurities and introduce the scattering rates $\tau^{-1}_{0/\boldsymbol{Q}} = 2\pi N_f u^2_{0/\boldsymbol{Q}}$ for non-magnetic impurities and $\left(\tau^p_{0/\boldsymbol{Q}}\right)^{-1} = 2\pi N_f \sum_i \left(\mathbf{u}^p_{0/\boldsymbol{Q}}\cdot\hat{\boldsymbol{e}}_i\right)^2$ for paramagnetic impurities. In the hot-spots model, the density of states is $N_f = \Lambda_\parallel/(2\pi)^2 v_F$, with $\Lambda_\parallel$ denoting the momentum cutoff parallel to the Fermi surface. We obtain:

$$
\begin{aligned}
Z^{-1}(\omega) =& 1 + \left(\frac{1}{2\tau_0} + \frac{1}{2\tau_{\boldsymbol{Q}}} + \frac{1}{2\tau_0^p} + \frac{1}{2\tau_{\boldsymbol{Q}}^p}\right) \frac{1}{\sqrt{\bar{\Delta}_\omega^2 + \omega^2}} && (4) \\
\bar{\Delta}_\omega =& -\frac{\bar{\Delta}_\omega}{\sqrt{\omega^2 + \bar{\Delta}_\omega^2}} \left(\frac{1}{\tau_{\boldsymbol{Q}}} + \frac{1}{\tau_0^p}\right) + V N_f \int_0^\Lambda \frac{\bar{\Delta}_\omega \mathrm{d}\omega}{\sqrt{\omega^2 + \bar{\Delta}_\omega^2}} && (5)
\end{aligned}
$$

From the last equation, it is clear that only the inter-hot-spot non-magnetic impurity and the intra-hot-spot paramagnetic impurity suppress the SC gap. The last equation can be solved self-consistently to find $\bar{\Delta}_\omega$; it is convenient then to define an effective SC order parameter given by:

$$
\Delta = V N_f \int_0^\Lambda \frac{\bar{\Delta}_\omega \mathrm{d}\omega}{\sqrt{\omega^2 + \bar{\Delta}_\omega^2}} \ .
$$

This is the quantity plotted in Fig. 4b of the main text.

Next, we consider how the SDW vertex Γ_{SDW} is dressed by impurity scattering. As shown in Fig. S3, the dressed SDW vertex can be conveniently written in Nambu space as:

$$
\Gamma_{\mathrm{SDW}} = \Gamma_{\mathrm{SDW}}^{\alpha} \left(\Psi_c^\dagger \sigma_0 \Psi_d + h.c.\right) - i \Gamma_{\mathrm{SDW}}^{\beta} \left(\Psi_c^\dagger \sigma_1 \Psi_d - h.c.\right)
$$

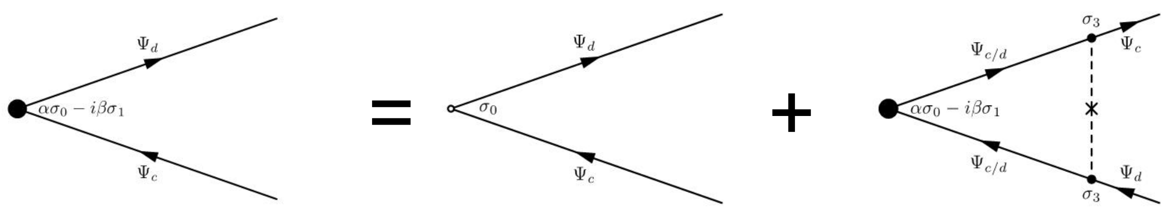

FIG. S3. The spin vertex dressed by the non-magnetic impurity scattering.

To calculate the dressed SDW vertex, we need to integrate over the two dimensional momentum. To calculate these integrals, we apply the transformation:

$$
\int \mathrm{d}^2\boldsymbol{k} \quad \Longrightarrow \quad \int \frac{\mathrm{d}\epsilon_c \mathrm{d}\epsilon_d}{|\boldsymbol{v}_c \times \boldsymbol{v}_d|} \tag{6}
$$

To simply the notation, we define the following quantities (see also Ref. [39]):

$$
\begin{aligned}
F_{\Delta^2} =& \frac{\omega(\omega+\Omega) + \bar{\Delta}_\omega \bar{\Delta}_{\omega+\Omega}}{\sqrt{\omega^2 + \bar{\Delta}_\omega^2}\sqrt{(\omega+\Omega)^2 + \bar{\Delta}_{\omega+\Omega}^2}} \\
F_{\omega\Delta} =& \frac{\omega \bar{\Delta}_{\omega+\Omega} - (\omega+\Omega)\bar{\Delta}_\omega}{\sqrt{\omega^2 + \bar{\Delta}_\omega^2}\sqrt{(\omega+\Omega)^2 + \bar{\Delta}_{\omega+\Omega}^2}} \\
\tau_{\mathrm{damping}}^{-1} =& N_f 4 |\boldsymbol{v}_c \times \boldsymbol{v}_d| = \frac{\Lambda_\parallel v_f \sin\theta}{\pi^2}
\end{aligned} \tag{7}
$$

Direct evaluation of the vertex functions gives the coupled equations:

$$
\begin{aligned}
\Gamma_{\mathrm{SDW}}^{\alpha} &= 1 + \tau_{\mathrm{damping}} \left[\left(\frac{1}{2\tau_0} + \frac{1}{2\tau_{\boldsymbol{Q}}}\right) - \frac{1}{3}\left(\frac{1}{2\tau_0^p} + \frac{1}{2\tau_{\boldsymbol{Q}}^p}\right)\right] \left(-\Gamma_{\mathrm{SDW}}^{\alpha} F_{\Delta^2} + \Gamma_{\mathrm{SDW}}^{\beta} F_{\omega\Delta}\right) \\
\Gamma_{\mathrm{SDW}}^{\beta} &= \tau_{\mathrm{damping}} \left[\left(\frac{1}{2\tau_0} - \frac{1}{2\tau_{\boldsymbol{Q}}}\right) + \frac{1}{3}\left(\frac{1}{2\tau_0^p} - \frac{1}{2\tau_{\boldsymbol{Q}}^p}\right)\right] \left(\Gamma_{\mathrm{SDW}}^{\alpha} F_{\omega\Delta} + \Gamma_{\mathrm{SDW}}^{\beta} F_{\Delta^2}\right)
\end{aligned} \tag{8}
$$

from which we can compute the magnetic susceptibility in Matsubara space:

$$\chi_{\mathrm{SDW}}(\boldsymbol{Q}, i\Omega) = N_f \tau_{\mathrm{damping}} \int \frac{\mathrm{d}\omega}{2\pi} \left(\Gamma^{\alpha}_{\mathrm{SDW}} F_{\Delta^2} - \Gamma^{\beta}_{\mathrm{SDW}} F_{\omega\Delta}\right) \tag{9}$$

Computing the static magnetic susceptibility ($\Omega = 0$) gives:

$$F_{\Delta^2} = 1\ , F_{\omega\Delta} = 0 \quad \Longrightarrow \quad \Gamma^{\alpha}_{\mathrm{SDW}} = \left[1 + \frac{\tau_{\mathrm{damping}}}{2}\left(\frac{1}{\tau} - \frac{1}{3}\frac{1}{\tau^p}\right)\right]^{-1} \tag{10}$$

where we defined the total non-magnetic scattering rate $\tau^{-1} = \tau_0^{-1} + \tau_{\boldsymbol{Q}}^{-1}$ and the total paramagnetic scattering rate $(\tau^p)^{-1} = (\tau_0^p)^{-1} + \left(\tau_{\boldsymbol{Q}}^p\right)^{-1}$. Note that the dressed SDW vertex becomes a constant, independent of the frequency ω. Clearly, while non-magnetic scattering always reduces $\chi_{\mathrm{SDW}}(\boldsymbol{Q}, 0)$, paramagnetic impurity scattering enhances it. In Fig. 4 of the main text, we considered the case of point-like impurities, in which $\tau_0^{-1} = \tau_{\boldsymbol{Q}}^{-1}$ and $(\tau_0^p)^{-1} = \left(\tau_{\boldsymbol{Q}}^p\right)^{-1}$.